Available online at www.sciencedirect.com
ScienceDirect
Trans. Nonferrous Met. Soc. China 32(2022) 2276−2289
Transactions of Nonferrous Metals Society of China
www.tnmsc.cn

Microstructure and properties of Cu−2Cr−1Nb alloy fabricated by spark plasma sintering

Ya-ke REN[1*], Xue-qian LÜ[1*], Zu-ming LIU[1], Bing WEI[1], Ting LEI[1], Quan LI[1], Xiao-bo JI[2], Wen-tao DENG[2], Yong-kang AI[1]

1. State Key Laboratory of Powder Metallurgy, Central South University, Changsha 410083, China;
2. School of Chemistry and Chemical Engineering, Central South University, Changsha 410083, China

Received 30 March 2020; accepted 18 March 2021

Abstract: Cu−2Cr−1Nb alloy was fabricated by spark plasma sintering (SPS) using close coupled argon-atomized alloy powder as the raw material. The optimal SPS parameters obtained using the $L_9(3^4)$ orthogonal test were 950 °C, 50 MPa and 15 min, and the relative density of the as-sintered alloy was 99.8%. The rapid densification of SPS effectively inhibited the growth of the Cr_2Nb phase, and the atomized powder microstructure was maintained in the grains of the alloy matrix. Uniformly distributed multi-scale Cr_2Nb phases with grain sizes of 0.10−0.40 μm and 20−100 nm and fine grains of alloy matrix with an average size of 3.79 μm were obtained. After heat treatment at 500 °C for 2 h, the room temperature tensile strength, electrical conductivity, and thermal conductivity of the sintered Cu−2Cr−1Nb alloy were 332 MPa, 86.7% (IACS), and 323.1 W/(m·K), respectively, and the high temperature tensile strength (700 °C) was 76 MPa.

Key words: Cu−Cr−Nb alloy; spark plasma sintering; Cr_2Nb phase; microstructure; properties

1 Introduction

As a kind of essential structural and functional material, Cu−Cr alloys with excellent strength and conductivity have been widely used in aerospace, energy, electronics, transportation, and other industries. Recently, many Cu−Cr alloys have been developed, such as Cu−Cr [1,2], Cu−Cr−Zr [3,4], Cu−Cr−Ag [5], Cu−Cr−Mg [6], and Cu-based matrix composites [7−10]. However, the application of many Cu−Cr alloys in aerospace is limited due to their poor softening resistance at elevated temperature. Adding alloying elements to form thermostable phases is an effective way to solve this problem. Cu−Cr−Nb alloys exhibit superior comprehensive properties, and are one of the structural and functional copper alloy materials with the greatest potential to meet the demands for strength, creep and fatigue resistance, thermal conductivity, and structural stability required in aerospace applications [11−22].

The number and size of Cr_2Nb phases and the grain size of alloy matrix play a vital role in the properties of the Cu−Cr−Nb alloys [23−26]. However, Cr and Nb easily form a coarsened intermetallic compound, Cr_2Nb, with high thermal stability, high melting point, and high elastic modulus during solidification of the melted alloy [12,21]. DHOKEY et al [27,28] prepared a Cu−8Cr−4Nb (at.%) alloy by casting, in which the second phase had a size of 0.7−7 μm and was mainly distributed at grain boundaries. GUO et al [29] regulated phase formation in cast Cu−0.47Cr−0.16Nb (wt.%) alloy by homogenizing annealing, cold rolling, and aging, and the average

* Ya-ke REN and Xue-qian LÜ contributed equally to this work
Corresponding author: Zu-ming LIU, Tel: +86-731-88836355/+86-13975809336, E-mail: lzm@csu.edu.cn
DOI: 10.1016/S1003-6326(22)65947-8

size of Cr_2Nb phase in the alloy was around 0.7 μm. YANG et al [30] prepared a novel Cu−2Cr−1.35Nb−0.15Zr (wt.%) alloy by drop casting, deformation processing, and heat treatment. The size of Cr_2Nb phase in this alloy was 0.3−1 μm, and the electrical conductivity was less than 60% (IACS) (International Annealed Copper Standard). To regulate the second phase and improve the properties, ELLIS and MICHAL [12] prepared a Cu−Cr−Nb alloy strip by chill block melt spinning (CBMS). The fine Cr_2Nb phase in the alloy strip was distributed uniformly in the matrix, but the conductivity of the alloy strip was less than 70% (IACS). Many researchers prepared Cu−8Cr−4Nb (at.%), Cu−4Cr−2Nb (at.%), and Cu−8Cr−4Nb (Zr) (at.%) alloys by hot extrusion (HE) [11,31], hot isostatic pressing (HIP) [21], vacuum hot pressing (VHP) [13,16,17,32−34], spark plasma sintering (SPS) [33], cold spraying [35], and plasma spraying [36] using the as-atomized alloy powder as the raw material.

The average size of the Cr_2Nb phases in the Cu−8Cr−4Nb and Cu−4Cr−2Nb alloys was about 0.93 and 0.78 μm, respectively, and the electrical conductivity of the alloys was less than 75% (IACS) for both. ANDERSON [11], SHUKLA et al [17,32,33], LOEWENTHAL and ELLIS [37], and VETTRAINO et al [38] further investigated the effects of deformation processing on the microstructure and properties of the Cu−8Cr−4Nb alloy. The results showed that the distribution of the Cr_2Nb phase in the hot-extruded/warm-rolled Cu−8Cr−4Nb alloy became more uniform with decrease of grain size compared with the hot-extruded alloy. However, the size of the Cr_2Nb phase was not significantly decreased. ANDERSON et al [11,24,39] and SHUKLA et al [33,40] regulated the microstructure of the atomized Cu−8Cr−4Nb and Cu−4Cr−2Nb alloy powder by mechanical alloying (MA). The size of the Cr_2Nb phase in the alloys fabricated with MA powder was decreased significantly, and the mechanical properties of the alloy were clearly improved, but the electrical conductivity of the alloy was reduced. In addition to meeting the demands for strength and thermal stability, there is also high requirement for conductivity for aerospace structural and functional materials. Reducing the contents of Cr and Nb can significantly improve the conductivity, but it easily causes to reduce the strength. Therefore, improving strength and conductivity of Cu−Cr−Nb alloy remains a challenge.

In this work, the Cu−2Cr−1Nb alloy was prepared by SPS using close-coupled argon-gas-atomized powder as the raw material. We expected that the size of the Cr_2Nb phase could be regulated by rapid densification, and excellent matching of strength and conductivity could be obtained via microstructure regulation.

2 Experimental

The Cu−2Cr−1Nb alloy was fabricated by SPS (HPD25−3, Germany) using close-coupled argon-gas-atomized powder as the raw material as described in detail in our previous work [41]. The microstructure of the Cu−2Cr−1Nb alloy powders is shown in Fig. 1. Figures 1(a, b) show the SEM images of the powders with cross-section diameters of about 31 and 32 μm, respectively. The white particles uniformly distributed in the alloy matrix with average sizes of 0.29 and 0.30 μm are part of Cr_2Nb phases, while no Cr_2Nb phase with microscale particles was observed, and only results for the statistical analysis of the visible Cr_2Nb phase in SEM images are given. The volume fraction of the second phase was about 3.5%. Figures 1(c, d) depict the TEM images of the atomized powders. The nanoscale and submicron Cr_2Nb phases were uniformly distributed in the matrix.

The sintering parameters were optimized by $L_9(3^4)$ orthogonal experiment, and the experimental factors including the sintering temperature, pressure, and time, are shown in Table 1. Relative density is an important parameter of powder metallurgical material that is related to its properties [42], and was also included as an evaluation index. The significance of the experimental factors was evaluated by the range (R), and K_i (i=1, 2, 3) was used to evaluate the experimental level of each factor. To reduce the influence of the solid solubility of Cr and Nb atoms on the performance evaluation of the sintered alloys, the sintered alloys were further heat-treated at 500 °C for 2 h.

The alloy microstructure was observed by field emission scanning electron microscope (SEM, Quanta FEG 250, Czech), electron backscatter

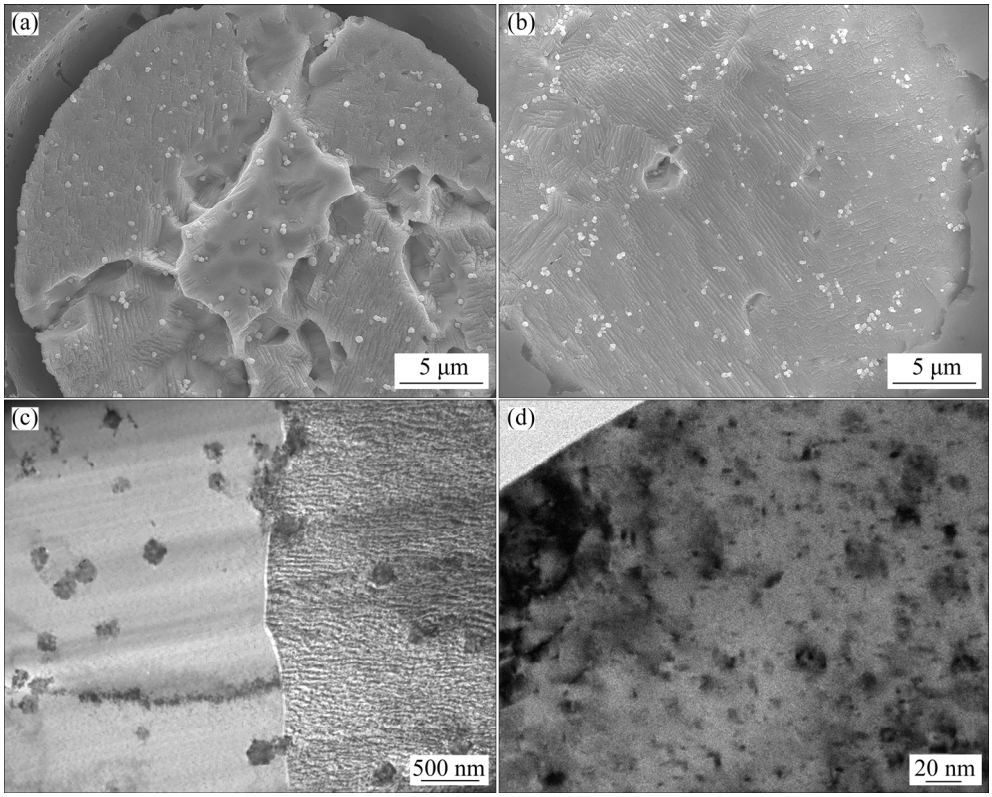

Fig. 1 Microstructures of gas-atomized Cu−2Cr−1Nb alloy powders: (a, b) SEM images of powders with diameters of about 31 and 32 μm, respectively; (c, d) TEM images of powder with diameter of about 20 μm

Table 1 Results of $L_9(3^4)$ orthogonal experiment and range analysis

Sample No.	Experimental parameter			Experimental result
	Sintering temperature/°C	Sintering pressure/MPa	Sintering time/min	Relative density/%
1	850	40	5	95.2
2	850	45	10	98.3
3	850	50	15	99.4
4	900	40	10	99.2
5	900	45	15	99.6
6	900	50	5	99.3
7	950	40	15	99.7
8	950	45	5	99.6
9	950	50	10	99.7
K_1	292.9	294.1	294.1	
K_2	298.1	297.5	297.2	
K_3	299	298.4	298.7	
R	6.1	4.3	4.6	

diffractometer (EBSD, FEG 650, Czech), and field emission transmission electron microscope (TEM, JEM−2100F, Japan), and the fracture morphology of the alloy was observed by SEM. The overall size of the second phase was statistically analyzed using the Nano Measurer 1.2 software using the SEM images, and the grain size was analyzed using the EBSD post-processing software HKL CHANNEL 5. The SEM samples were prepared by hot-mounting and standard metallographic technique and etched

by $FeCl_3$ reagent. The EBSD and TEM samples of the alloy were prepared using electrolytic double spray thinner (Tenupol−5, Denmark) with a voltage of 20.5 V, an etching solution of 24 vol.% nitric acid−methanol solution, and a temperature from −40 to −30 °C.

The relative densities of the sintered alloys were converted from the measured and theoretical densities. The theoretical density of the Cu−2Cr−1Nb (at.%) alloy was 8.89 g/cm^3, and the measured density was tested by the Archimedes principle and taken from the average value of three samples. According to ISO 6892 [43,44], the alloy tensile properties were tested using an electronic universal testing machine (Instron 3369, USA) at 25 and 700 °C, respectively, and the strain rate was 1.0 mm/min. The electrical conductivity of the alloy was measured using a digital conductivity meter (D60 K, China).

The thermal conductivity was measured by a laser thermal conductivity meter (ZDJR−3, Germany), which was taken from the average value of three samples with the same preparation state. Based on the thermal conductivity data of five groups of samples prepared under different conditions, a linear equation between the thermal conductivity and electrical conductivity was established, which was y=−49.77+4.30x, fitting coefficient R_1=0.973, where x is the electrical conductivity (% (IACS)) and y is the thermal conductivity (W/(m·K)), and the thermal conductivity of the other samples was obtained using the above linear equation.

3 Results and discussion

3.1 Orthogonal experiment results

As indicated by the experimental results and range R analysis in Table 1, the order of R followed R_T>R_t>R_p (where T, p, and t are the sintering temperature, pressure, and time, respectively). It was demonstrated that the sintering temperature had the most significant effect on the relative density of alloy, followed by the sintering time and then pressure; thus, the effect of sintering temperature should be given priority. K_i in Table 1 shows that increasing the temperature and pressure and extending the sintering time of SPS were beneficial to the densification of the alloy powder and obtaining a higher relative density. As a result, the optimal sintering temperature, pressure, and time for SPS were 950 °C, 50 MPa, and 15 min, respectively. The relative density of the as-sintered Cu−2Cr−1Nb alloy was reached 99.8%, which is higher than that of the Cu−8Cr−4Nb alloy [33].

The Cu−2Cr−1Nb alloy powder was densified by the particle rearrangement, plastic rheology and diffusion bonding [42,45]. An increase in sintering temperature effectively reduces the deformation resistance of the powder, increases the diffusion rate of atoms (which is conducive to the formation and growth of the sintering neck), and promotes powder densification. The sintering parameters (including the sintering temperature, time, and pressure) have essential effects on the powder densification. The sintering temperature mainly affects the atom thermal motion and diffusion and the powder deformation resistance; increasing sintering time is conducive to the powder densification process and improves the alloy relative density. The sintering pressure affects the rearrangement, plastic rheology, and plastic deformation of the alloy powder [42].

The sintering temperature has a significant effect on the thermal movement rate and diffusivity of the atom as well as the deformation resistance of the powder. The thermal movement rate and the diffusivity of the matrix atom were low, while the deformation resistance of the powder was high at low temperature. At a low sintering pressure and a short sintering time, the sufficient rearrangement, plastic rheology, and plastic deformation of the powder were difficult to realize, and the atom diffusion and powder densification were insufficient. Therefore, the relative density of the alloy prepared by the sintering parameters of 850 °C, 40 MPa and 5 min was low (95.2%). By contrast, increasing the sintering temperature significantly promoted the atom diffusion.

Compared with those at 850 °C, the volume diffusion coefficient and the surface diffusion coefficient of the copper atom at 950 °C increased by about 540% and 114%, respectively [46], the thermal movement of atoms was accelerated, and the deformation resistance of powder was reduced. Low powder deformation resistance and high sintering pressure were beneficial to promoting the powder rearrangement, plastic rheology, and plastic deformation, resulting in the elimination of porosity, enlargement of the contact area between the powder and atomic diffusion channel, and promotion of

metallurgical bonding at the powder interface. By extending the sintering time, the diffusion of atoms and the densification of the alloy powder were more sufficient. As a result, Cu−2Cr−1Nb alloy prepared at 950 °C, 50 MPa and 15 min achieved a higher relative density of up to 99.8%.

3.2 Microstructure of as-sintered Cu−2Cr−1Nb alloy

Figure 2 shows the XRD patterns of the gas-atomized Cu−2Cr−1Nb alloy powder and as-sintered alloy prepared at 950 °C, 50 MPa and 15 min. Three diffraction peaks related to the copper matrix were observed in XRD pattern of as-sintered alloy. According to the standard PDF card of copper (PDF No. 04-836), it was found that the diffraction peak of copper shifted to a small angle, which indicates that some of the Cr and Nb elements exist in the form of solid solution atoms in as-sintered alloy. Compared with the gas-atomized alloy powder, the intensity of the copper diffraction peaks was reduced, and the number and intensity of the diffraction peaks of the Cr_2Nb phase were increased, which indicates that fresh Cr_2Nb phase was precipitated from the matrix during the SPS process.

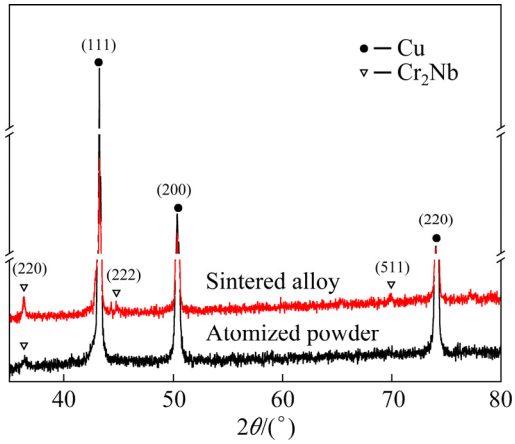

Fig. 2 XRD patterns of gas-atomized powder and as-sintered Cu−2Cr−1Nb alloy prepared at 950 °C, 50 MPa and 15 min

Figure 3(a) depicts the SEM image of as-sintered alloy prepared at 850 °C, 40 MPa and 5 min. There were some sintering defects (irregular pores and prior particle boundaries) in the matrix, most of the sintering necks did not grow, and the alloy powders were not deformed. Figure 3(b) shows a locally enlarged observation of Fig. 3(a) (based on the square area indicated by the arrow), indicating the prior particle boundaries and the

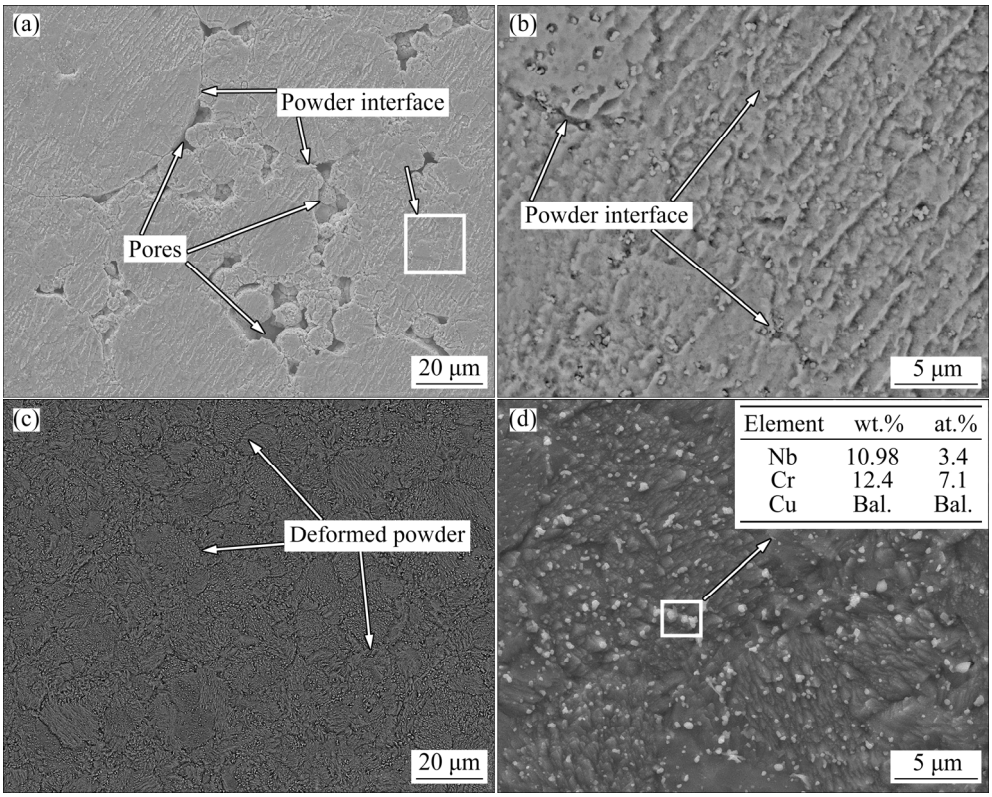

Fig. 3 SEM images of as-sintered Cu−2Cr−1Nb alloy prepared at 850 °C, 40 MPa and 5 min (a, b), and 950 °C, 50 MPa and 15 min (c, d)

uniformly distributed second phase with an average size of 0.31 μm. The results indicate that powder densification was incomplete at 850 °C, 40 MPa and 5 min, which resulted in a lower relative density (95.2%).

Figures 3(c, d) show the SEM observation results of the Cu−2Cr−1Nb alloy prepared at 950 °C, 50 MPa and 15 min, which show that the sintering defects were evidently reduced. No noticeable pores were observed, the bonding state of the prior particle boundaries was significantly improved, and some powders were clearly deformed (Fig. 3(c)). The submicron second phase with a size of less than 0.40 μm (the average size of about 0.32 μm) was distributed homogeneously in the matrix (Fig. 3(d)). The EDS analysis results show that the submicron second phase was mainly composed of Cr and Nb (the arrow region in Fig. 3(d)), and the molar ratio of Cr to Nb was 2:0.8. The above results suggest that the sintering parameters had a significant effect on the alloy microstructure. Increasing the sintering temperature, pressure and time favors reducing or even eliminating the sintering defects. In addition, the size of second phase in the as-sintered alloy did not obviously increase.

The EBSD image and grain size distribution of as-sintered alloy prepared at 950 °C, 50 MPa and 15 min are shown in Fig. 4. Most of the grains in the matrix are deformed grains, and only a few are near-equiaxed grains (Fig. 4(a)), suggesting that powder densification was achieved by plastic rheology and deformation of the powder. The equivalent diameter of matrix grains was 2−12 μm, and the average grain size was 3.79 μm (Fig. 4(b)), which has no obvious change compared with the atomized powder, given that rapid densification of SPS and the Cr_2Nb phase can inhibit grain coarsening.

The TEM observation results for the Cu−2Cr−1Nb alloy prepared at 950 °C, 50 MPa and 15 min are shown in Fig. 5. The spherical nanophase with a size of 20−100 nm (the average size of 69 nm) was also uniformly distributed in the alloy matrix, in addition to the submicron phase with a size of 0.1−0.3 μm, shown in Figs. 5(a, b); however, the number of nanophases was decreased. The EDS results indicate that the molar ratio of Cr to Nb in the nanophase indicated in Fig. 5(a) was 1.92:1 (shown in Fig. 5(c)), which corresponds to Cr_2Nb. The large second phase (Region *A* in Fig. 5(b)) was analyzed by selected area electron diffraction (SAED) as shown in Fig. 5(d). The calibration results show that it was a FCC (face centered cubic) structure, with interplanar spacing related to the (200) plane of 0.3428 nm and a lattice constant of 0.6856 nm.

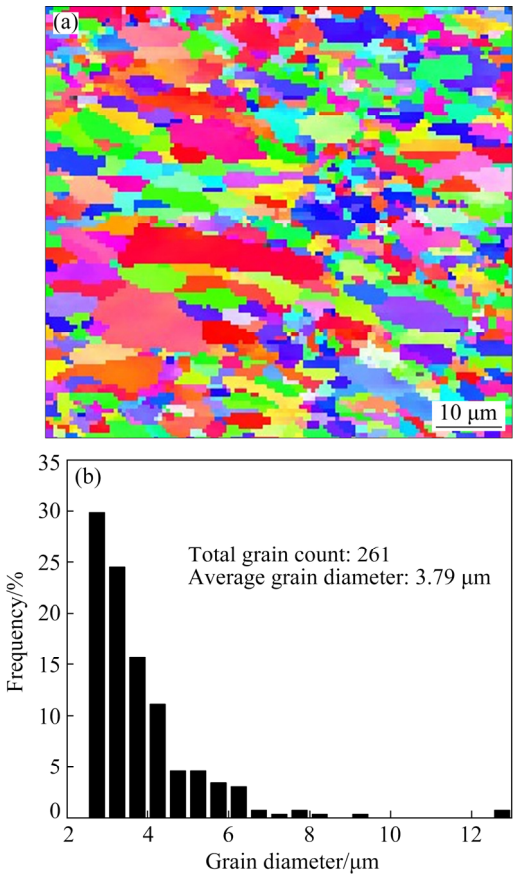

Fig. 4 EBSD image (a) and grain size distribution (b) of as-sintered Cu−2Cr−1Nb alloy prepared at 950 °C, 50 MPa and 15 min

The high-resolution transmission electron microscopy (HRTEM) images of Regions *B* and *C* in Fig. 5(b) are shown in Figs. 5(e, f), respectively. A clear phase interface can be observed between the matrix and the second phase, and the Fourier transform of the HRTEM image (arrow region) shows that the small second phase was also a FCC structure, with interplanar spacings of 0.3528, 0.4107, 0.4054, and 0.2476 nm corresponding to crystal planes of $(\bar{2}00)$, $(\bar{1}1\bar{1})$, $(11\bar{1})$, and $(\bar{2}\,\bar{2}0)$, respectively, and the lattice constants of 0.7063 (Fig. 5(e)) and 0.7002 nm (Fig. 5(f)). Combining the results of the XRD, EDS, SAED, and HRTEM, the second phase in as-sintered alloy was mainly Cr_2Nb phase with a FCC structure.

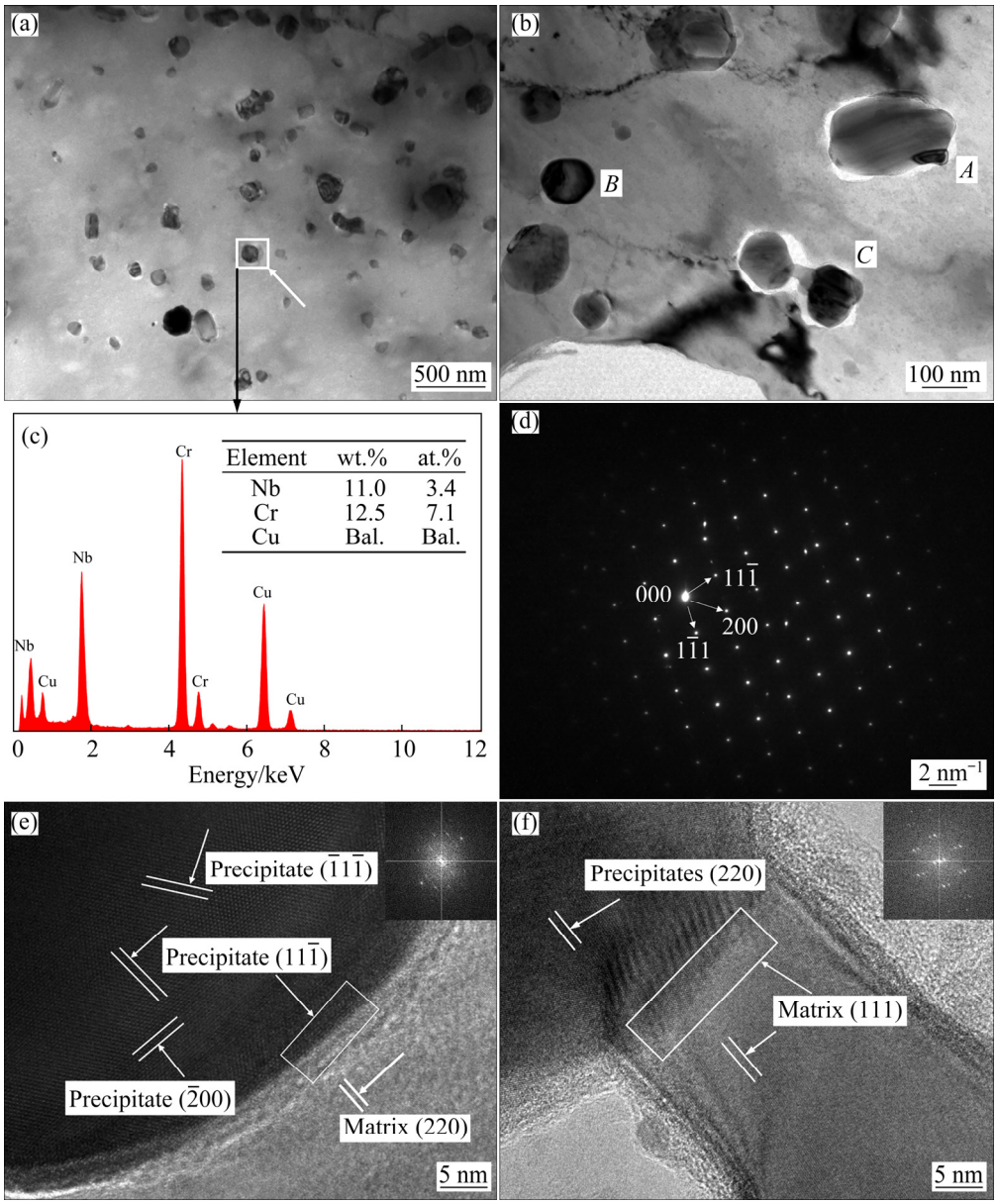

Fig. 5 Microstructures of as-sintered Cu−2Cr−1Nb alloy prepared at 950 °C, 50 MPa and 15 min: (a, b) TEM images; (c) EDS pattern; (d) SAED pattern of Region *A* in (b); (e, f) HRTEM images of Regions *B* and *C* in (b), respectively

Figure 6 shows the HAADF-STEM image and corresponding element mapping of the Cu−2Cr−1Nb alloy prepared at 950 °C, 50 MPa and 15 min. Most of the Cr and Nb elements were enriched to form the second phase, and only some were distributed in the copper matrix.

The formation and growth of the Cr_2Nb phase were inhibited and a supersaturated solid solution was obtained by rapid solidification of the close-coupled argon gas atomization (10^4−10^6 K/s) [41,47,48], while some Cr and Nb were precipitated from the supersaturated solid solution to form the fine Cr_2Nb phase during the SPS process (Fig. 2). At the same time, the concentrations of Cr and Nb atoms in the small particles of the Cr_2Nb phase were higher than those in the large particles of the Cr_2Nb phase, resulting in the concentration gradient of Cr and Nb in the matrix, which provided suitable thermodynamical conditions for coarsening of the Cr_2Nb phase. Correspondingly, the amount of the Cr_2Nb phase was reduced and the size was increased, especially for the nano-Cr_2Nb phases (Figs. 5(a, b)).

The growth rate of the Cr_2Nb phase was controlled by the Nb diffusivity in the copper matrix, which was less than 4.11×10^{-12} cm^2/s, and

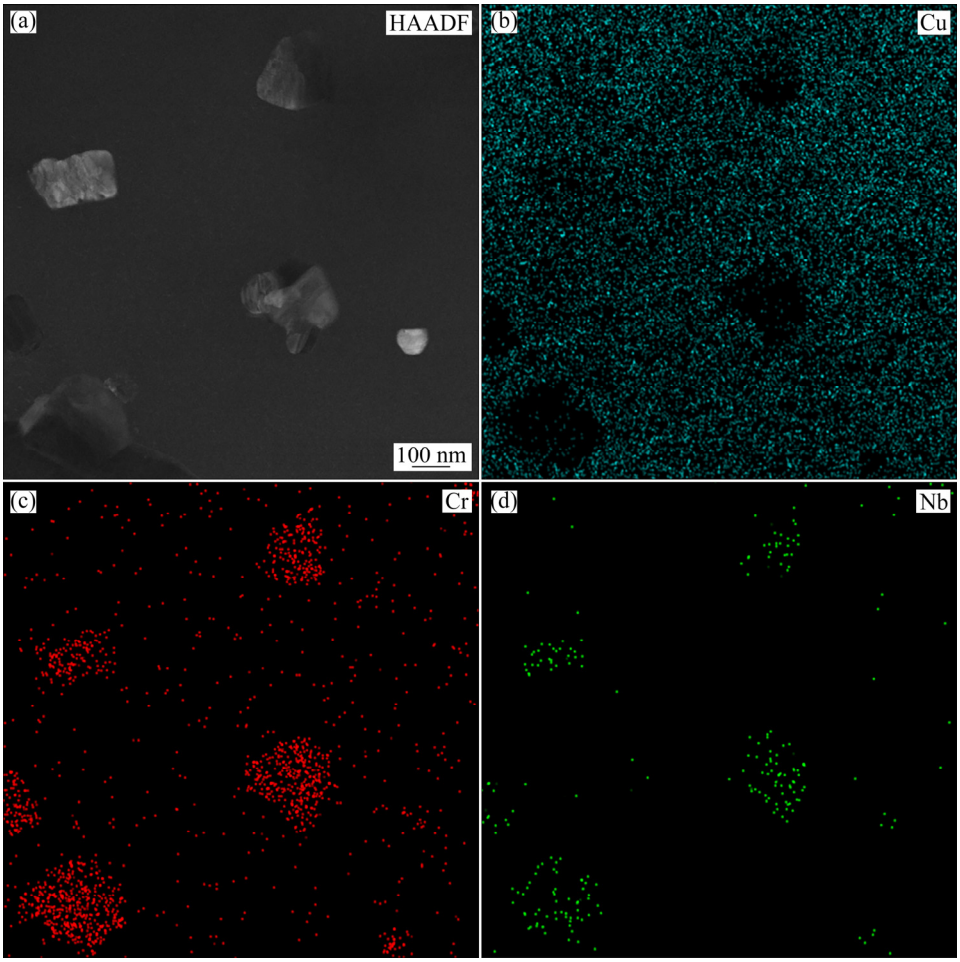

Fig. 6 HAADF-STEM image of as-sintered Cu−2Cr−1Nb alloy prepared at 950 °C, 50 MPa and 15 min (a) and its elemental distribution (b−d)

the average size of the Cr_2Nb phase in as-sintered Cu−2Cr−1Nb alloy prepared at 850 °C, 40 MPa and 5 min was increased to 0.31 μm (shown in Fig. 2(b)) from 0.30 μm (as-atomized powder in Figs. 1(a, b)). Changing the sintering parameters to 950 °C, 50 MPa and 15 min, the diffusivity of Nb in the copper matrix was about 4.08×10^{-11} cm^2/s, which was 993% of that of Nb at 850 °C [46]; however, the size of the Cr_2Nb phase was only increased to 0.32 μm (from 0.30 μm). This was attributed to the rapid densification and short sintering time (15 min) of SPS as well as the excellent thermal stability of Cr_2Nb. Therefore, overcoarsening of the Cr_2Nb phase was effectively inhibited by the rapid densification of SPS and the microstructure of the as-atomized Cu−2Cr−1Nb alloy powder was maintained. The Cr_2Nb phase in the Cu−2Cr−1Nb alloy was finer than that in the reported Cu−8Cr−4Nb [11,32], Cu−4Cr−2Nb [11], and Cu−8Cr−4Nb (Zr) [31] alloys.

3.3 Properties of alloys

Table 2 shows the properties of Cu−2Cr−1Nb alloy prepared by SPS and SPS + heat treatment. This demonstrates that with the increase in the sintering temperature and pressure, the tensile strength of the sintered alloy was enhanced, while the electrical and thermal conductivities were declined. As can be seen from Table 2, The as-sintered alloy with optimal comprehensive properties prepared at 950 °C, 50 MPa and 15 min exhibited tensile strength, electrical conductivity, and thermal conductivity of 324 MPa, 64.3% (IACS), and 226.7 W/(m·K), respectively.

Temperature had crucial effects on the solid solubility of Cr and Nb atoms in the copper matrix. At 850−950 °C (0.83−0.92 times the T_m of copper), the Cr and Nb atom solid solubilities at 950 °C were higher than those at 850 °C [48], and the precipitation of the solid solution Cr and Nb atoms was inhibited by the high cooling rate of SPS.

Table 2 Properties of Cu−2Cr−1Nb alloys prepared by SPS and SPS + heat treatment (HT) at 500 °C for 2 h

Sample No.	Sintering parameter			Property					
	Temperature/ °C	Pressure/ MPa	Time/ min	Tensile strength/MPa		Electrical conductivity/ % (IACS)		Thermal conductivity/(W·m^{-1}·K^{-1})	
				SPS	SPS+HT	SPS	SPS+HT	SPS	SPS+HT
1	850	40	5	247	262	64.5	76.2	227.6	277.9
2	850	45	10	306	308	70.0	82.7	251.2	305.8
3	850	50	15	313	320	71.0	85.2	255.5	316.6
4	900	40	10	314	314	67.7	84.2	241.3	312.3
5	900	45	15	316	323	67.7	86.1	241.3	320.5
6	900	50	5	310	317	69.1	84.7	247.4	314.4
7	950	40	15	315	328	65.1	86.5	230.2	322.2
8	950	45	5	319	329	66.9	86.3	237.9	321.3
9	950	50	10	311	331	65.5	86.2	231.9	320.9
10	950	50	15	324	332	64.3	86.7	226.7	323.1

Therefore, the solid solubilities of the Cr and Nb atoms were higher in as-sintered alloy prepared at higher temperature which, in turn, greatly affected the properties of as-sintered alloys, particularly the electrical conductivity and thermal conductivity [49].

Table 2 shows the properties of the sintered alloys heat-treated at 500 °C for 2 h. The tensile strength, electrical conductivity and thermal conductivity of the alloy prepared by SPS at 850 °C, 40 MPa and 5 min and heat treatment were 262 MPa, 76.2% (IACS), and 277.9 W/(m·K), respectively. There was an improvement in alloy properties with the increase in the sintering temperature, pressure, and time. The tensile strength, electrical conductivity, and thermal conductivity of the alloy prepared by SPS at 900 °C, 45 MPa and 15 min and heat treatment were 23.3%, 13%, and 15.3% higher than those of the alloy prepared by SPS at 850 °C, 40 MPa and 5 min and heat treatment, respectively.

The alloy prepared by SPS with the optimum parameters followed by heat treatment exhibited tensile strength, electrical conductivity, and thermal conductivity of 332 MPa, 86.7% (IACS), and 323.04 W/(m·K), respectively (these results were reported in our other paper [50]), which were 26.7%, 13.8%, and 16.3% higher than those of the alloy prepared by SPS at 850 °C, 40 MPa and 5 min and subsequent heat treatment, respectively. The sintering parameters significantly affected the properties and relative density, and high temperature, high pressure, and a long sintering time comprehensively favored an improvement in alloy properties.

The performances of the Cu−2Cr−1Nb, Cu−8Cr−4Nb [11,17,32,51,52], and Cu−4Cr−2Nb alloys [11] are compared in Table 3. After heat treatment at 500 °C for 2 h, the electrical conductivity of the Cu−2Cr−1Nb alloy was 60.6%, 15.6%, and 17.2% higher than those of the HE/aged Cu−8Cr−4Nb, VHP/aged Cu−8Cr−4Nb, and Cu−4Cr−2Nb alloys, respectively. The tensile strength was similar to that of the Cu−4Cr−2Nb alloy at room temperature, and reached 76 MPa at 700 °C, which was higher than that of the VHP/aged Cu−8Cr−4Nb alloy.

Figure 7 shows the stress−strain curves of the as-sintered Cu−2Cr−1Nb alloy. The sintering temperature had a significant influence on the plasticity of the Cu−2Cr−1Nb alloy, and the increase in sintering temperature improved the elongation of the alloy. The elongation of the alloy prepared by SPS at 950 °C (Sample 10) was higher than that at 850 °C (Sample 1), which was mainly caused by the reduction of sintering defects and increase of relative density of the alloy with the increase in sintering temperature (Fig. 2 and Table 1).

Figure 8 shows the fracture morphologies of the Cu−2Cr−1Nb alloys prepared by SPS. As shown in Figs. 8(a, b), many prior particles and irregular pores were observed in the Cu−2Cr−1Nb alloy prepared at 850 °C, 40 MPa and 5 min, and

Table 3 Performance comparison of Cu−Cr−Nb alloys

Alloy	Processing method	Tensile strength/MPa		Electrical conductivity/% (IACS)	Ref.
		25 °C	700 °C		
Cu−8Cr−4Nb	Argon gas atomization + HE + aging	426	100	54	[11,24,51,52]
	Argon gas atomization + VHP + aging	400	72	75	[17,32]
Cu−4Cr−2Nb	Argon gas atomization + HE + aging	325	75	74	[11,24]
Cu−2Cr−1Nb	Close-coupled argon atomization + SPS + aging	332	76	86.7	This work

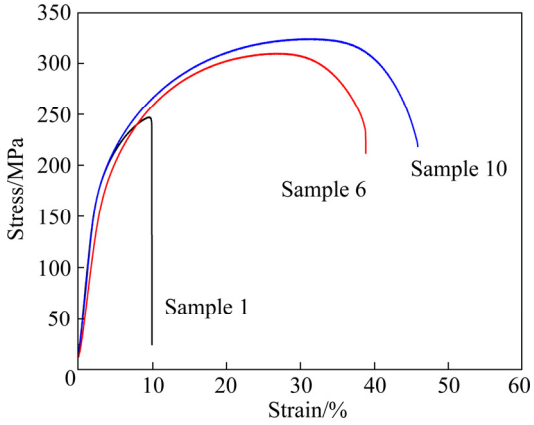

Fig. 7 Stress–strain curves of as-sintered Cu−2Cr−1Nb alloy

there were only a small number of dimples along the sintered neck. By contrast, no prior particles and irregular pores were observed on the fracture surface of the Cu−2Cr−1Nb alloy prepared at 950 °C, 50 MPa and 15 min (Fig. 8(c)), and a large number of fractured dimples were observed (Fig. 8(d)), which collectively represent prominent characteristics of ductile failure.

The microstructure of the Cu−2Cr−1Nb alloy, including the sintering defects, grain size, and Cr_2Nb phase, is the key factor affecting its mechanical properties. As shown in Fig. 3(a) and Figs. 8(a, b), there were many sintering defects in the alloy prepared by SPS at 850 °C, 40 MPa and 5 min, which was easy to cause stress concentration and lead to the generation and propagation of cracks, thus reducing the tensile strength. Therefore, the sintering defect was vital in determining the strength for the alloy prepared at low temperature, low pressure and short time. The significant increase in strength (332 MPa) of the alloy prepared at 950 °C, 50 MPa and 15 min is attributed to the reduction of sintering defects (Fig. 3(c)). In this case, the mechanical properties were mainly controlled by the grain size of the matrix as well as the number and size of the Cr_2Nb phase.

The grain boundary strengthening and the precipitation strengthening are the main strengthening mechanisms of the Cu−2Cr−1Nb alloy. According to the grain size (3.79 μm, Fig. 4), the strength contribution from grain boundary strengthening was calculated to be 81 MPa. The precipitation strengthening is related to the Cr_2Nb phase, which has a higher elastic modulus compared with the copper matrix and is not easy to deform. Therefore, the dislocations bypassed the Cr_2Nb phase particles and formed dislocation loop, which further inhibited the subsequent movement of dislocations and improved the strength. The strengthening effect could be expressed using the Orowan−Ashby equation shown as follows [11,25,53]:

$$\Delta\sigma_{\text{Orowan}}=\frac{0.84MGb}{2\pi(1-\upsilon)^{0.5}\left(r\sqrt{\frac{2\pi}{3f}}-2r\right)}\ln\frac{r}{b}\approx\alpha f^{0.5}r^{-1} \quad (1)$$

where $\Delta\sigma_{\text{Orowan}}$ is the Orowan-calculated component of the yield strength, M is the Taylor factor, G is the shear modulus, b is the Burgers vector component, υ is the Poisson ratio of the copper matrix, α is a constant, r is the average radius, and f is the volume fraction of the second phase. By using the values of G, b, and υ as 45.5 GPa, 0.256 nm, and 0.343 for copper, the strength contribution from the submicron Cr_2Nb phase (the average size of 0.32 μm) was calculated to be 37 MPa, and this was 45 MPa from the nanophase (the average size of 69 nm) to the total yield strength. The calculated yield strength of the sintered alloy prepared at 950 °C, 50 MPa and 15 min was 163 MPa, which was 10% lower than the measured value of 181 MPa.

From Eq. (1), the Orowan strengthening effect ($\Delta\sigma_{\text{Orowan}}$) was determined by the size and volume fraction of the second phase. This is in positive proportion to the volume fraction and in inverse

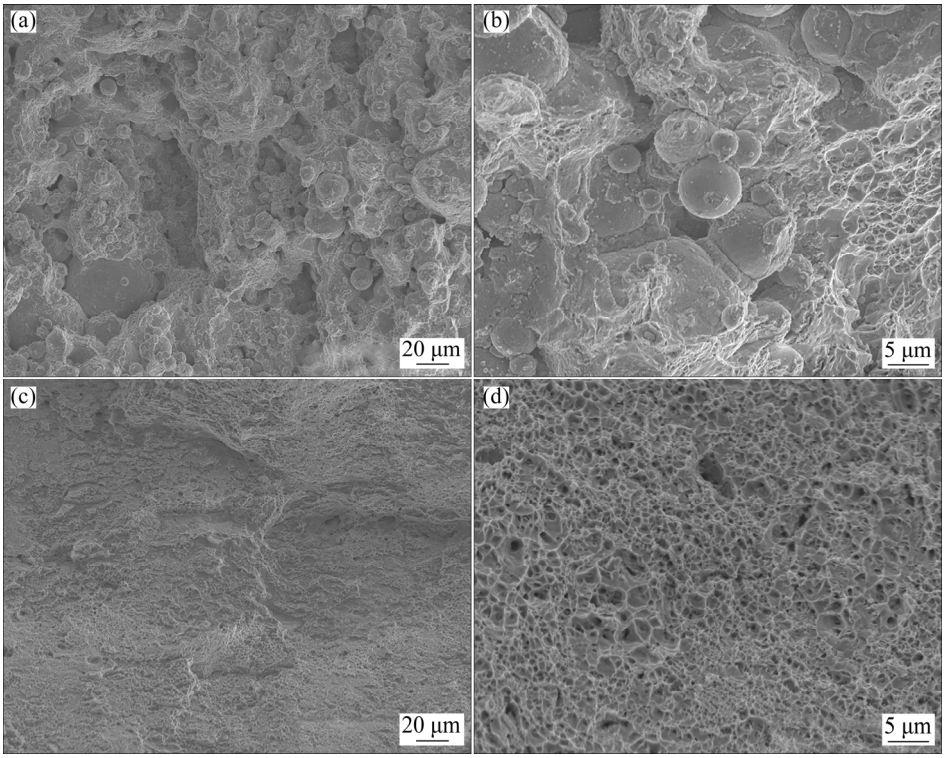

Fig. 8 Fracture morphologies of Cu−2Cr−1Nb alloys prepared at 850 °C, 40 MPa and 5 min (a, b), and 950 °C, 50 MPa and 15 min (c, d)

proportion to the size of the second phase, and the size of the second phase contributes more to $\Delta\sigma_{\text{Orowan}}$. In terms of the calculated contents of Cr and Nb, the Cr_2Nb phase volume fraction in the Cu−2Cr−1Nb alloy was about 3.5%, which was only about 25% and 50% of that in the Cu−8Cr−4Nb and Cu−4Cr−2Nb alloys, respectively, and $\Delta\sigma_{\text{Orowan}}$ was decreased by 50% and 29.3%.

However, the average size of the Cr_2Nb phase in the Cu−2Cr−1Nb alloy prepared at 950 °C, 50 MPa and 15 min was 0.32 μm (shown in Fig. 3), which was about 34.4% and 41% of that in the Cu−8Cr−4Nb and Cu−4Cr−2Nb alloys, respectively [11], and the $\Delta\sigma_{\text{Orowan}}$ was increased by 191% and 144%. The $\Delta\sigma_{\text{Orowan}}$ of Cu−2Cr−1Nb alloy was increased by 45% and 72.5%, respectively, compared with that of the Cu−8Cr−4Nb and Cu−4Cr−2Nb alloys. The Orowan strengthening effect of the Cr_2Nb phase in the Cu−2Cr−1Nb alloy was increased, and its room temperature tensile strength was similar to that of the Cu−4Cr−2Nb alloy [11,24].

The Cr_2Nb phase with good stability not only hindered the dislocation climb but also inhibited the grain boundary slip at elevated temperature. The strong hindrance to the dislocation climb and grain boundary slip could be obtained via a large amount of second phase with small size. While the volume fraction of the Cr_2Nb phase in the Cu−2Cr−1Nb alloy was lower than that in the Cu−8Cr−4Nb and Cu−4Cr−2Nb alloys, the size of the Cr_2Nb phase was found to have clearly decreased. Therefore, the tensile strength of the sintered Cu−2Cr−1Nb alloy at 700 °C was similar to that of the Cu−4Cr−2Nb alloy and 5.5% higher than that of the hot-pressed/aged Cu−8Cr−4Nb alloy.

The electrical and thermal conductivities of metals are controlled by free-motion electrons and are positively correlated with the electron free path. The electron free path is affected by defects, such as impurities, interfaces, phonons, and dislocations, and the relationship between the total resistivity of the alloy and the resistivity of each component is shown in the following equation [11,32]:

$$\rho_{\text{total}}=\rho_{\text{dislocation}}+\rho_{\text{phonon}}+\rho_{\text{interface}}+\rho_{\text{impurities}} \quad (2)$$

where ρ_{total} is the total resistivity of the alloy, $\rho_{\text{dislocation}}$ is the resistivity component induced by dislocations, ρ_{phonon} is the resistivity component due to phonons, $\rho_{\text{interface}}$ is the resistivity component induced by the interface (including the sintering defects, grain boundary, and the interface between

the second phase and matrix), and $\rho_{impurities}$ is the resistance induced by impurities, especially solution atoms.

As the Cu−2Cr−1Nb alloy prepared in this work did not undergo deformation processing, the resistivity components $\rho_{dislocation}$ and ρ_{phonon}, caused by dislocations and phonons, respectively, could be ignored at room temperature [11]. The grain boundary contribution to the $\rho_{interface}$ of the Cu−2Cr−1Nb alloy prepared with different sintering parameters was the same as the sintered alloy had similar grain size.

The sintering defects, solid solution Cr and Nb, and Cr_2Nb phase are the key factors affecting the electrical and thermal conductivities of the alloy. The resistivity component $\rho_{interface}$ in Eq. (2) contributes the most to ρ_{total}. For the Cu−2Cr−1Nb alloy prepared at 850 °C, 40 MPa and 5 min, a large number of sintering defects (Figs. 3(a, b)), which have a strong electron scattering effect [54,55], resulted in a low electrical conductivity (64.5% (IACS)).

The Cu−2Cr−1Nb alloy prepared at 950 °C, 50 MPa and 15 min showed fewer sintering defects (Figs. 3(c, d)), but the higher sintering temperature of the SPS resulted in higher solid solubilities of Cr and Nb (Fig. 6), which led to low conductivity of 64.3% (IACS). The $\rho_{impurities}$ reduced with the decrease of the solid solubilities of Cr and Nb after heat treatment at 500 °C for 2 h. Therefore, the electrical conductivity was increased from 64.3% (IACS) to 86.7% (IACS), which was higher than that of the alloy prepared by SPS at 850 °C, 40 MPa and 5 min and subsequent heat treatment (76.2% (IACS)). Compared with the Cu−8Cr−4Nb and Cu−4Cr−2Nb alloys [11], the interfaces between the second phase and the matrix in the Cu−2Cr−1Nb alloy were much smaller due to the smaller volume fraction of the second phase, which led to a lower value of the resistivity component $\rho_{interface}$. As a result, the electrical and thermal conductivities of the Cu−2Cr−1Nb alloy were significantly increased.

4 Conclusions

(1) High temperature and pressure promoted densification of the Cu−2Cr−1Nb (at.%) alloy powder. The as-sintered alloy fabricated with the optimum parameters (950 °C, 50 MPa and 15 min) had a relative density of 99.8%.

(2) The SPS rapid densification suppressed the overcoarsening of the grain and Cr_2Nb phase. The average grain size of sintered alloy matrix was 3.79 μm, and the Cr_2Nb phase with a multi-scale size of 0.10−0.50 μm and 20−100 nm was uniformly distributed.

(3) The tensile strength, electrical conductivity, and thermal conductivity of the sintered alloy heat-treated at 500 °C for 2 h were 332 MPa, 86.7% (IACS), and 323.1 W/(m·K) at room temperature, respectively, and the tensile strength at high temperature (700 °C) was 76 MPa. These suggest that a good agreement between the strength and conductivity of the Cu−Cr−Nb alloy was obtained through SPS parameter optimization.

Acknowledgments

This work was financially supported by the National Key Research and Development Program of China (No. 2016YFB0301300), Innovation Driven Project of Central South University, China (No. 2015CX004), State Key Laboratory of Powder Metallurgy, Central South University, China, and the Open Fund of National Joint Engineering Research Center for Abrasion Control and Molding of Metal Materials, China (No. HKDNM201907).

References

[1] HE Wen-xiong, YU Yang, WANG Er-de, SUN Hong-fei, HU Lian-xi, CHEN Hui. Microstructures and properties of cold drawn and annealed submicron crystalline Cu−5%Cr alloy [J]. Transactions of Nonferrous Metals Society of China, 2009, 19(1): 93−98.

[2] ZHANG Sha-sha, ZHU Hai-hong, ZHANG Luo, ZHANG Wen-qi, YANG Huan-qing, ZENG Xiao-yan. Microstructure and properties of high strength and high conductivity Cu−Cr alloy components fabricated by high power selective laser melting [J]. Materials Letters, 2019, 237: 306−309.

[3] FU Hua-dong, XU Sheng, LI Wei, XIE Jian-xin, ZHAO Hong-bin, PAN Zhi-jun. Effect of rolling and aging processes on microstructure and properties of Cu−Cr−Zr alloy [J]. Materials Science and Engineering A, 2017, 700: 107−115.

[4] PAN Zhen-ya, CHEN Jiang-biao, LI Jin-fu. Microstructure and properties of rare earth-containing Cu−Cr−Zr alloy [J]. Transactions of Nonferrous Metals Society of China, 2015, 25: 1206−1214.

[5] XU Sheng, FU Hua-dong, WANG Ying-tao, XIE Jian-xin. Effect of Ag addition on the microstructure and mechanical properties of Cu−Cr alloy [J]. Materials Science and Engineering A, 2018, 726: 208−214.

[6] ZHAO Zi-qian, XIAO Zhu, LI Zhou, MA Mu-zhi, DAI Jie. Effect of magnesium on microstructure and properties of Cu−Cr alloy [J]. Journal of Alloys and Compounds, 2018, 752: 191−197.

[7] LI Zi-li, WANG Wei-min, WANG Ji-lin. Effects of TiB_2 on microstructure of nano-grained Cu−Cr−TiB_2 composite powders prepared by mechanical alloying [J]. Advanced Powder Technology, 2014, 25(1): 415−422.

[8] HAMEDAN S S, ABDI M, SHEIBANI S. Comparative study on hot rolling of Cu−Cr and Cu−Cr−CNT nanocomposites [J]. Transactions of Nonferrous Metals Society of China, 2018, 28: 2044−2052.

[9] CHAKRABORTY S, GUPTA A K, ROY D, BASUMALLICK A. Studies on nano-metal dispersed Cu−Cr matrix composite [J]. Materials Letters, 2019, 257: 126739.

[10] CHAKRABORTY S, BAGALA R, SIKDAR K, ROY D, BASUMALLICK A. Structure property relationship in a bulk Cu−Cr−W composite synthesized by high-energy ball milling and spark plasma sintering [J]. Materials Chemistry and Physics, 2020, 256: 123708.

[11] ANDERSON K R. Effects of thermal and mechanical processing on microstructures and desired properties of particle-strengthened Cu−Cr−Nb alloys [R]. Cleveland, Ohio: NASA, 2000.

[12] ELLIS D L, MICHAL G M. Precipitation strengthened high strength, high conductivity Cu−Cr−Nb alloys produced by chill block melt spinning [R]. Cleveland, Ohio: NASA, 1989.

[13] SHUKLA A K, NARAYANA MURTY S V S, SHARMA S C, MONDAL K. Densification behavior and mechanical properties of Cu−Cr−Nb alloy powders [J]. Materials Science and Engineering A, 2012, 551: 241−248.

[14] ANDERSON K R. High temperature coarsening of Cr_2Nb precipitates in Cu−8Cr−4Nb alloy [R]. Cleveland, Ohio: NASA, 1996.

[15] SHUKLA A K, NARAYANA MURTY S V S, SHARMA S C, MONDAL K. The serrated flow and recrystallization in dispersion hardened Cu−Cr−Nb alloy during hot deformation [J]. Materials Science and Engineering A, 2016, 673: 135−140.

[16] SHUKLA A K, SAMUEL M G, NARAYANA MURTY S V S, SHARMA S C, MONDAL K. Effect of powder oxidation on densification and properties of vacuum hot pressed Cu−Cr−Nb alloy [J]. Materials Science and Engineering A, 2013, 561: 452−459.

[17] SHUKLA A K, SURESH KUMER R, NARAYANA MURTY S V S, MONDAL K. Enhancement of high temperature ductility of hot-pressed Cu−Cr−Nb alloy by hot rolling [J]. Materials Science and Engineering A, 2013, 577: 36−42.

[18] DEGROH H C, ELLIS D L, LOEWENTHAL W S. Comparison of GRCop-84 to other Cu alloys with high thermal conductivities [J]. Journal of Materials Engineering and Performance, 2008, 17(4): 594−606.

[19] SHUKLA A K, SHARMA V M J, NARAYANA MURTY S V S, NARAYANA MURTY P R, SHARMA S C. Integrity of structural and thermo-structural materials for Indian space programme [J]. Procedia Engineering, 2014, 86: 8−17.

[20] ASRAFF A K, APARNA R, KUMARESAN D. Comparison of creep properties of four copper alloys and creep based stress analysis of a rocket engine combustion chamber [J]. Procedia Engineering, 2013, 55: 45−50.

[21] ELLIS D L. GRCop-84: A high-temperature copper alloy for high-heat-flux applications [R]. Cleveland, Ohio: NASA, 2005.

[22] ELLIS D L, LOEWENTHAL W S. Tensile properties of GRCop-84 [R]. Cleveland, Ohio: NASA, 2012.

[23] TIAN Bao-hong, SONG Ke-xing, LIU Ping. High performance dispersion strengthened copper matrix composite and its preparation technology [J]. Beijing: Science Press, 2011: 1−30. (in Chinese)

[24] ANDERSON K R, GROZA J R. Microstructural size effects in high-strength high-conductivity Cu−Cr−Nb alloys [J]. Metallurgical and Materials Transactions A, 2001, 32: 1211−1224.

[25] GROZA J R, GIBELING J C. Principles of particle selection for dispersion strengthened copper [J]. Materials Science and Engineering A, 1993, 171: 115−125.

[26] HAZZLEDINE P M. Direct versus indirect dispersion hardening [J]. Scripta Metallurgica et Materialia, 1992, 26: 57−58.

[27] DHOKEY N B, SARVE S N, LAMSOGE H A. Development of in-situ synthesis of Cr_2Nb reinforced copper alloy by aluminothermic process [J]. Transactions of the Indian Institute of Metals, 2011, 64(4−5): 425−429.

[28] DHOKEY N B, SARVE S N, LAMSOGE H A. In-situ synthesis of Cr_2Nb reinforced copper alloy by liquid metallurgy route [J]. Materials Science Forum, 2012, 710: 143−148.

[29] GUO Xiao-li, XIAO Zhu, QIU Wen-ting, LI Zhou, ZHAO Zi-qian, WANG Xu, JIANG Yan-bin. Microstructure and properties of Cu−Cr−Nb alloy with high strength, high electrical conductivity and good softening resistance performance at elevated temperature [J]. Materials Science and Engineering A, 2019, 749: 281−290.

[30] YANG Ying, WANG Ling, SNEAD L, ZINKLE S J. Development of novel Cu−Cr−Nb−Zr alloys with the aid of computational thermodynamics [J]. Materials & Design, 2018, 156: 370−380.

[31] ELLIS D L, LERCH B A. Improvement of GRCop-84 through the addition of zirconium [R]. Cleveland, Ohio: NASA, 2012.

[32] SHUKLA A K, NARAYANA MURTY S V S, SHARMA S C, MONDAL K. Aging behavior and microstructural stability of a Cu−8Cr−4Nb alloy [J]. Journal of Alloys and Compounds, 2014, 590: 514−525.

[33] SHUKLA A K, NARAYANA MURTY S V S, SHARMA S C, MONDAL K. Effect of hot rolling on the enhancement of mechanical properties of low density Cu−Cr−Nb sintered alloy [J]. Materials & Design, 2013, 43: 125−133.

[34] SHUKLA A K, NRARAYANA MURTY S V S, SHARMA S C, MONDAL K. Constitutive modeling of hot deformation behavior of vacuum hot pressed Cu−8Cr−4Nb alloy [J]. Materials & Design, 2015, 75: 57−64.

[35] LI Wen-ya, GUO Xue-ping, DEMBINSKI L, LIAO Han-lin, CODDET C. Effect of vacuum heat treatment on microstructure and microhardness of cold sprayed Cu−4Cr−2Nb alloy coating [J]. Transactions of Nonferrous Metals Society of China, 2006, 16(S): s203−s208.

[36] LI Wen-ya, GUO Xue-ping, VERDY C, DEMBINSKI L. Improvement of microstructure and property of cold-sprayed Cu−4at.%Cr−2at.%Nb alloy by heat treatment [J]. Scripta Materialia, 2006, 55: 327−330.
[37] LOEWENTHAL W S, ELLIS D L. GRCop-84 rolling parameter study [R]. Cleveland, Ohio: NASA, 2008.
[38] VETTRAINO L G, HEELAN J L, FACONTI C A, WALLEY J L, GARG A, GROZA J R, GIBELING J C. Influence of processing on the microstructure of Cu−8Cr−4Nb [J]. Journal of Materials Science, 2008, 43(19): 6546−6555.
[39] ANDERSON K R, GROZA J R, ULMER D G. Microstructural refinement and strengthening of Cu−4Cr−2Nb alloy by mechanical milling [J]. Scripta Materialia, 1997, 37(2): 179−185.
[40] SHUKLA A K, NARAYANA MURTY S V S, SHARMA S C, MONDAL K. Effect of powder milling on mechanical properties of hot-pressed and hot-rolled Cu−Cr−Nb alloy [J]. Journal of Alloys and Compounds, 2013, 580: 427−434.
[41] LV Xue-qian, LIU Zu-ming, LEI Ting, LI Quan. Microstructure and properties of Cu−Cr−Nb alloy powder prepared by argon gas atomization [J]. Advanced Powder Technology, 2019, 30(11): 2464−2472.
[42] HUANG Pei-yun. Principle of powder metallurgy [M]. Beijing: Metallurgical Industry Press, 2013: 370−410. (in Chinese)
[43] Metallic materials−Tensile testing. Part 1: Method of test at elevated temperature: ISO 6892—2: 2018 [S]. Switzerland: ISO International, 2018.
[44] Metallic materials−Tensile testing. Part 2: Method of test at room temperature: ISO 6892—1: 2019 [S]. Switzerland: ISO International, 2019.
[45] ORRÙ R, LICHERI R, LOCCI A M, CINCOTTI A, CAO G. Consolidation/synthesis of materials by electric current activated/assisted sintering [J]. Materials Science and Engineering R, 2009, 63(4/5/6): 127−287.
[46] BUTRYMOWWICZ D B. Diffusion rate data and mass transport phenomena for copper systems [M]. Washington: National Bureau of Standard, 1977: 18−146.
[47] LAVERNIA E J, SRIVATSAN T S. The rapid solidification processing of materials: Science, principles, technology, advances, and applications [J]. Journal of Materials Science, 2010, 45(2): 287−325.
[48] LIU X J, JIANG Z P, WANG C P, ISHIDA K. Experimental determination and thermodynamic calculation of the phase equilibria in the Cu−Cr−Nb and Cu−Cr−Co systems [J]. Journal of Alloys and Compounds, 2009, 478: 287−296.
[49] MIYAKE J, GHOSH G, FINE M E. Design of high-strength, high-conductivity alloys [J]. MRS Bulletin, 1996, 21(6): 13−18.
[50] LV Xue-qian, LIU Zu-ming, LEI Ting, LI Quan, REN Ya-ke, ZHOU Xu, ZHANG Ze-jie. Effect of heat treatment on Cr_2Nb phase and properties of spark plasma sintered Cu−2Cr−1Nb alloy [J]. Materials, 2020, 13(12): 2860.
[51] ANDERSON K R, GROZA J R, DRESHFIELD R L, ELLIS D L. High performance dispersion-strengthened Cu−8Cr−4Nb alloy [J]. Metallurgical and Materials Transactions A, 1995, 26: 2197−2206.
[52] GROZA J R. Microstructural features of a new precipitationstrengthened Cu−8Cr−4Nb alloy [J]. Materials Characterization, 1993, 31: 133−141.
[53] ZHENG Zi-qiao. Fundamentals of the materials science [M]. 2nd ed. Changsha: Central South University Press, 2013, 493−498. (in Chinese)
[54] MONTES J M, CUEVAS F G, CINTAS J. Porosity effect on the electrical conductivity of sintered powder compacts [J]. Applied Physics A, 2008, 92(2): 375−380.
[55] MONTES J M, RODRÍGUEZ J A, HERRERA E J. Thermal and electrical conductivities of sintered powder compacts [J]. Powder Metallurgy, 2003, 46(3): 251−256.

放电等离子烧结 Cu−2Cr−1Nb 合金的显微组织与性能

任亚科[1]，吕学谦[1]，刘祖铭[1]，魏 冰[1]，雷 霆[1]，李 全[1]，纪效波[2]，邓文韬[2]，艾永康[1]

1. 中南大学 粉末冶金国家重点实验室，长沙 410083；
2. 中南大学 化学化工学院，长沙 410083

摘 要：以紧耦合氩气雾化合金粉末为原料，采用放电等离子烧结(SPS)制备 Cu−2Cr−1Nb 合金。通过 $L_9(3^4)$正交试验优化得到的最优 SPS 参数为 950 ℃、50 MPa 和 15 min，所制备合金的相对密度为 99.8%。SPS 快速致密化有效地抑制 Cr_2Nb 相长大，并保持雾化粉末的基体组织，获得分布均匀、尺度为 0.10~0.40 μm 和 20~100 nm 的多尺度 Cr_2Nb 相以及平均尺寸为 3.79 μm 的基体晶粒。经 500 ℃、2 h 热处理所制备 Cu−2Cr−1Nb 合金的室温抗拉强度、电导率和热导率分别达到 332 MPa、86.7% (IACS) 和 323.1 W/(m·K)，高温抗拉强度(700 ℃) 为 76 MPa。

关键词：Cu−Cr−Nb 合金；放电等离子烧结；Cr_2Nb 相；显微组织；性能

(Edited by Wei-ping CHEN)